Journal of the Optical Society of America B
OPTICAL PHYSICS

Substrate-mediated lattice Kerker effect in Al metasurfaces

A. S. Kostyukov,[1,*] A. E. Ershov,[1,2] R. G. Bikbaev,[1,3] V. S. Gerasimov,[1,2] I. L. Rasskazov,[4] S. V. Karpov,[1,3] and S. P. Polyutov[1]

[1]International Research Center of Spectroscopy and Quantum Chemistry—IRC SQC, Siberian Federal University, Krasnoyarsk 660041, Russia
[2]Institute of Computational Modelling of the Siberian Branch of the Russian Academy of Sciences, Krasnoyarsk 660036, Russia
[3]L. V. Kirensky Institute of Physics, Federal Research Center KSC SB RAS, Krasnoyarsk 660036, Russia
[4]The Institute of Optics, University of Rochester, Rochester, New York 14627, USA
*Corresponding author: askostyukov@sfu-kras.ru

Received 16 April 2021; revised 21 June 2021; accepted 23 June 2021; posted 23 June 2021 (Doc. ID 427939); published 15 July 2021

Surface lattice resonances (SLRs) emerging in regular arrays of plasmonic nanoparticles (NPs) are known to be exceptionally sensitive to the homogeneity of the environment. It is considered necessary to have a homogeneous environment for engineering narrowband SLRs, while in a half-space environment, SLRs rapidly vanish as the contrast between the refractive indices of the substrate and superstrate increases. From this conventional wisdom, it is apparent that the delicate lattice Kerker effect emerging from SLRs and resonances on constituent NPs should be difficult to achieve in a non-homogeneous environment. Using a rigorous theoretical treatment with multipolar decomposition, we surprisingly find and explain a narrowband substrate-mediated lattice Kerker effect in two-dimensional arrays of Al nanocylinders in a half-space geometry. We propose to use this effect for sensing applications and demonstrate its broad tunability across the UV/Vis wavelength range.

https://doi.org/10.1364/JOSAB.427939

1. INTRODUCTION

In recent years, two-dimensional periodic arrays of plasmonic and dielectric nanoparticles (NPs) have attracted great interest due to their unique properties. These structures exhibit so-called surface lattice resonances (SLRs) [1–12] arising from the interaction of the localized resonance of a single particle (localized surface plasmon resonances in plasmonic and Mie resonances in all-dielectric NPs) and the Wood–Rayleigh lattice anomalies [13,14]. SLRs manifest themselves as narrow spectral lines with an exceptionally high Q-factor [5,6,15–17]. A fairly simple technology for manufacturing such two-dimensional structures, as well as an understanding of the control mechanisms of their optical properties, made it possible to use SLRs in narrowband light absorption [18], sensorics [19], lasers [20–23], upconversion [24,25], and fluorescence [26–29] enhancement.

The interaction between SLRs with electric and magnetic resonances of different orders allows to observe the lattice Kerker effect, comprehensively studied in dielectric structures exhibiting strong electric dipole (ED) and magnetic dipole (MD) and quadrupole resonances: in single particles [30,31] and in arrays [32–35]. This effect is poorly studied in plasmonic structures due to their weak magnetic response, with rare exceptions of Au [36] and Al [37] NP arrays. Recently, aluminum has been increasingly used instead of conventional plasmonic materials such as silver and gold [38,39], particularly for SLRs in two-dimensional NP arrays [28,40–44]. However, all these works are limited to either ED or ED and electric quadrupole (EQ) interactions. Recently, we have shown that Al NPs support relatively strong MD and magnetic quadrupole (MQ) resonances compared to conventional plasmonic materials [45]. This feature is of critical importance for harnessing the lattice Kerker effect in arrays of plasmonic Al NPs [37], originating from the interaction between SLRs and resonances localized on single NPs.

SLRs are extremely sensitive to any perturbations in the homogeneity of the surrounding medium, for instance, high-Q SLRs are quite difficult [46,47] (yet possible under very certain circumstances [48–50]) to demonstrate in a half-space environment. This feature apparently makes it difficult to observe the lattice Kerker effect in arrays of NPs embedded in a non-homogeneous medium. Surprisingly, we show below that the half-space medium provides favorable conditions for a delicate interaction between the substrate and NPs enabling a narrowband *substrate-mediated* lattice Kerker effect [51]. Using rigorous numerical simulations along with multipole decomposition, we explicitly demonstrate the critical role of the substrate in mediating the lattice Kerker effect. Furthermore, we suggest to use a low-cost Al-based NP array as an optical sensor in the UV/Vis range with 263 nm/RIU sensitivity.

2. METHODS

A. Simulation Setup

A sketch of the considered structure is shown in Fig. 1(a) for a homogeneous environment and in Fig. 3(a) for a half-space geometry. A regular 2D array of Al cylinders with radius R and height H is located on the Si substrate. The periods of the array are p_x and p_y along x and y axes, respectively. The tabulated values of dielectric constants of aluminum [52] are used.

The total field $\mathbf{E}$ and the reflectance spectra of the described structures are calculated with the commercial finite-difference time-domain (FDTD) package [53]. Nanostructures are illuminated from the top by the plane wave with normal incidence along z axis and polarization along x axis. Reflection is calculated at the top of the simulation box. Perfectly matched layer boundary conditions are used on top and bottom sides, while the periodic boundary conditions are applied at the lateral boundaries of the simulation box. An adaptive mesh is used to reproduce accurately the nanodisk shape.

B. Multipole Decomposition

The electric far field scattered by any arbitrary object and found by any available numerical method (in our case, the FDTD method as described above) can be decomposed into dipole and quadrupole contributions [Chap. 9 54]. In our particular case, from the general considerations, we also explicitly add a contribution of a substrate:

$$\begin{aligned}\mathbf{E}_{sc} = &-\frac{\omega^2}{c^2 r_0}([[\mathbf{d}\times\mathbf{n}]\times\mathbf{n}] - [\mathbf{m}\times\mathbf{n}] \\ &- \frac{i\omega}{6c}([[\mathbf{D}\times\mathbf{n}]\times\mathbf{n}] - [\mathbf{M}\times\mathbf{n}]))e^{ikr_0} \\ &+ \frac{ik^2 c}{\omega}[\mathbf{n}\times[\mathbf{A}_s\times\mathbf{n}]]. \end{aligned} \tag{1}$$

Here r_0 is the distance to the observation point, $\mathbf{n}$ is the unit vector pointing to the observation point, ω is the frequency, $k = \omega/c$ is the wave vector, $\mathbf{d}$ and $\mathbf{m}$ are ED and MD, respectively, and $\mathbf{A}_s$ is the vector potential of the field mediated by the substrate. Cartesian components of EQ and MQ are $\mathbf{D} = \hat{D}\mathbf{n}$, $\mathbf{M} = \hat{M}\mathbf{n}$.

ED and MD and quadrupole moments induced on NP are defined as [54,55]

$$\begin{aligned}\mathbf{d} &= \iiint_{V_p}\left(\mathbf{P}j_0(kr) + \frac{k^2}{2(kr)^2}\left(3(\mathbf{P}\cdot\mathbf{r})\mathbf{r} - r^2\mathbf{P}\right)j_2(kr)\right)\mathrm{d}^3\mathbf{r}, \\ \mathbf{m} &= i\frac{k}{2}\iiint_{V_p}[\mathbf{P}\times\mathbf{r}]\frac{j_1(kr)}{kr}\mathrm{d}^3\mathbf{r}, \\ \hat{D} &= \iiint_{V_p}\left(\left(3\,(\mathbf{P}\otimes\mathbf{r} + \mathbf{r}\otimes\mathbf{P}) - 2(\mathbf{P}\cdot\mathbf{r})\hat{I}\right)\frac{j_1(kr)}{kr}\right. \\ &\quad \left. + 2k^2\left(5\mathbf{r}\otimes\mathbf{r}(\mathbf{P}\cdot\mathbf{r}) - (\mathbf{P}\otimes\mathbf{r} + \mathbf{r}\otimes\mathbf{P})\,r^2 - (\mathbf{P}\cdot\mathbf{r})\hat{I}\right)\right) \\ &\quad \times\frac{j_3(kr)}{(kr)^3}\mathrm{d}^3\mathbf{r}, \\ \hat{M} &= \frac{1}{3}ik\iiint_{V_p}(\mathbf{r}\otimes[\mathbf{P}\times\mathbf{r}] + [\mathbf{P}\times\mathbf{r}]\otimes\mathbf{r})\,\frac{j_2(kr)}{(kr)^2}\mathrm{d}^3\mathbf{r}, \end{aligned} \tag{2}$$

while a vector potential of the field created by the substrate is

$$\mathbf{A}_s = \frac{e^{ikr_0}}{cr_0}\iiint_{V_s}\mathbf{J}e^{-ik(\mathbf{n}\cdot\mathbf{r})}\mathrm{d}^3\mathbf{r}. \tag{3}$$

Here ε is the permittivity of NPs, $\mathbf{P} = (\varepsilon - 1)/4\pi\mathbf{E}$ is a polarization density, $\mathbf{J} = -i\omega\mathbf{P}$ is the current density, j_n are spherical Bessel functions of the first kind, $\hat{I}$ is a unit tensor, $r = |\mathbf{r}|$, and V_p and V_s distinguish integration over NPs and a substrate, respectively. The integration in Eq. (3) is performed numerically over a sufficiently thick (yet finite) part of a substrate just below an array of NPs. The numerical integration is terminated once $\mathbf{A}_s$ remains almost a constant as a function of increasing V_s with a predefined accuracy, sufficient for reported results to be reliable.

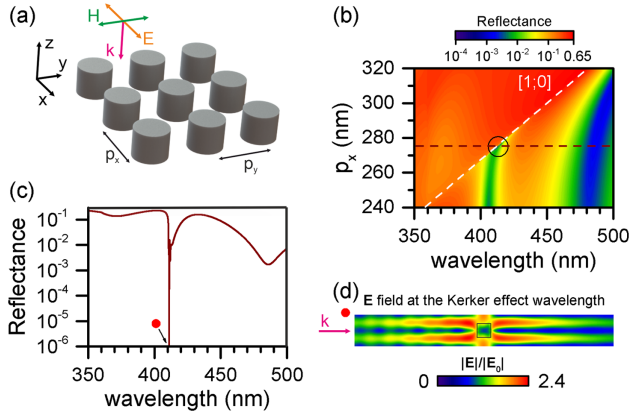

Fig. 1. (a) Sketch of 2D array of Al NPs in a homogeneous environment. Reflectance spectra of arrays with (b) fixed $p_y = 240$ nm and different p_x and (c) $p_y = 240$ nm and $p_x = 276.4$ nm, corresponding to the horizontal dashed line in (b). (d) Electric field distribution in xz plane at $\lambda_K = 411$ nm, corresponding to the Kerker effect [highlighted circle in (b) and red circle in (c)].

3. RESULTS AND DISCUSSION

A. Arrays in Homogeneous Environment

Before going into detail, it is instructive to discuss briefly the optical response of 2D Al NPs array embedded in a homogeneous medium with $\varepsilon_h = 2.25$ (optical glass). We consider cylinders with a fixed radius, $R = 60$ nm, and height, $H = 120$ nm, and calculate the reflection spectra of the two-dimensional structure. The simulation results are shown in Fig. 1(b). Narrowband suppression of the reflection can be observed by varying one of the periods while keeping the other one constant. In particular, the variation of p_x keeping $p_y = \text{const}$ yields control of the [1; 0] Rayleigh anomaly (RA) $\lambda_{\mathrm{RA}} = \sqrt{\varepsilon_h}p_x$, while varying the lattice period in the orthogonal direction leads to adjusting the [0; 1] RA [56,57], $\lambda_{\mathrm{RA}} = \sqrt{\varepsilon_h}p_y$. Similar to the case of spherical NPs [37], a complete suppression of reflection is observed at

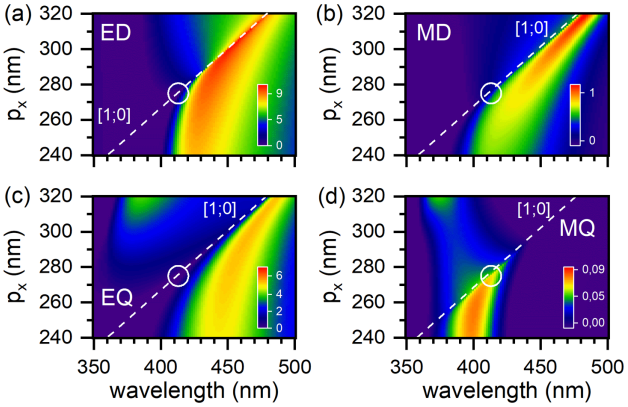

Fig. 2. Multipole decomposition of extinction efficiency, Q_{ext}, for arrays in Fig. 1(b): (a) ED, (b) MD, (c) EQ, and (d) MQ. See Eq. (4) for details. White dashed lines correspond to a spectral position of [1; 0] RA, $\lambda_{\text{RA}} = \sqrt{\varepsilon_h}\, p_x$, and highlighted circles are the same as in Fig. 1(b).

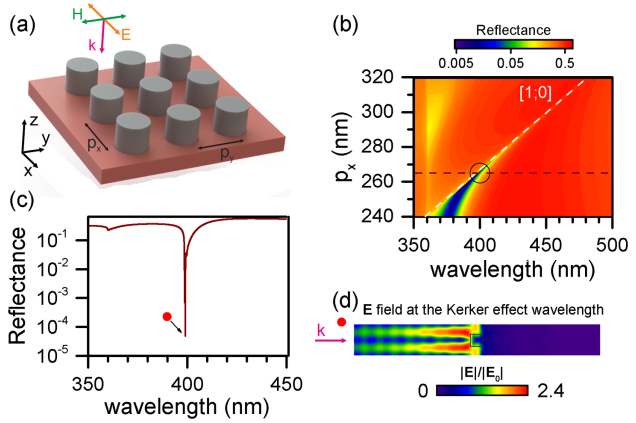

Fig. 3. (a) Sketch of 2D array of Al NPs on a substrate. Reflectance spectra of the structure with (b) fixed $p_y = 240$ nm and different p_x and (c) $p_y = 240$ nm and $p_x = 265.6$ nm, corresponding to the horizontal dashed line in (b). (d) Electric field distribution in xz plane at $\lambda_K = 400$ nm, corresponding to the Kerker effect [highlighted circle in (b) and red circle in (c)].

$\lambda_K = 411$ nm for arrays of cylindrical NPs with $p_x = 276.4$ nm and $p_y = 240$ nm [Fig. 1(c)]. Importantly, unlike the case of spherical NPs, an additional suppression band emerges in the range from 465 nm to 490 nm [Fig. 1(b)]. The amplitude of the electric field in the xz plane for the unit cell of the array at $\lambda_K = 411$ nm wavelength, which corresponds to zero reflection, is shown in Fig. 1(d). It can be seen that the electric field is enhanced near NPs, while the amplitude of the far field vanishes along the z axis.

The suppression of reflection at the Kerker effect wavelength, λ_K, can be explained with multipole decomposition (Fig. 2). The respective extinction cross sections are defined as

$$\sigma_{\text{ext;ED}} = \frac{4\pi k}{\sqrt{\varepsilon_h}|\mathbf{E}_0|^2}\Im(\mathbf{E}_0^* \cdot \mathbf{d}),$$

$$\sigma_{\text{ext;MD}} = \frac{4\pi k}{\sqrt{\varepsilon_h}|\mathbf{H}_0|^2}\Im(\mathbf{H}_0^* \cdot \mathbf{m}),$$

$$\sigma_{\text{ext;EQ}} = -\frac{\pi k}{3\sqrt{\varepsilon_h}|\mathbf{E}_0|^2}\Im\left[(\nabla \otimes \mathbf{E}_0^* + \mathbf{E}_0^* \otimes \nabla) : \hat{D}\right],$$

$$\sigma_{\text{ext;MQ}} = -\frac{2\pi k}{\sqrt{\varepsilon_h}|\mathbf{H}_0|^2}\Im\left[(\nabla \otimes \mathbf{H}_0^* + \mathbf{H}_0^* \otimes \nabla) : \hat{M}\right]. \quad \textbf{(4)}$$

Here $\mathbf{E}_0$ and $\mathbf{H}_0$ are components of the incident electromagnetic field, and ε_h is the permittivity of the medium that the incident light is impinging from. The respective extinction efficiency Q_{ext} is defined as the extinction cross section σ_{ext} normalized to the geometric cross section πR^2 of a single nanocylinder with radius R. As in the case of spherical NPs [37], the ED, MD, and EQ modes play the key role in the emergence of the lattice Kerker effect, while the contribution of the MQ mode is an order of magnitude smaller [Fig. 2(d)].

B. Arrays on Si Substrate

Consider similar 2D lattices of Al nanocylinders, but on a silicon substrate [Fig. 3(a)], with a superstrate having the same $\varepsilon_h = 2.25$ as in the previous subsection. Such structures are quite easy to manufacture, but the presence of the interface near nanocylinders can lead to partial or complete suppression of SLRs [46,47], and as a consequence, a vanishing of the Kerker effect due to the phase mismatch between the wave scattered from the NPs and the substrate. To investigate the influence of the substrate on the Kerker effect, we calculated the reflection spectra similar to Fig. 1(b), but for arrays on the Si substrate [Fig. 3(b)]. It can be seen that the half-space environment significantly changes the optical response of arrays of NPs. In contrast to the structures in a homogeneous environment (Fig. 1), the presence of a substrate provides a higher reflection coefficient at $\lambda > 420$ nm. In other words, in this wavelength range, such a structure acts almost like a mirror. Nonetheless, the Kerker effect is preserved, which is seen from the suppression of the reflection at $\lambda_K = 400$ nm for $p_x = 265.6$ nm [Fig. 3(c)]. The respective field distribution at the Kerker effect wavelength is shown in Fig. 3(d). The field profile in this case is similar to the field distribution in arrays embedded in a homogeneous medium [Fig. 1(d)], with the only difference that the field does not penetrate into the substrate in Fig. 3(d).

To understand nontrivial interaction of the electromagnetic fields in the NP array with the substrate, we plot multipole decomposition (ED, MD, EQ, MQ) of the amplitudes and phases of the reflected field in Figs. 4(a) and 4(b). Unlike the total suppression of backscattering due to the destructive interference of ED and MD + EQ resonances in NP arrays immersed in a homogeneous environment [37], the amplitudes of MD and EQ resonances are too low compared with ED [Fig. 4(a)]. Moreover, the phase difference [Fig. 4(b)] between multipoles cannot lead to full suppression of the reflection. The critical role of the substrate in emergence of the Kerker effect is clearly seen in Figs. 4(b) and 4(c). Indeed, the π-phase difference [Fig. 4(b)] between the field mediated by NPs and the field reflected by the substrate only along with equal values of their amplitudes [Fig. 4(c)] at $\lambda_K \approx 400$ nm leads to full suppression of the backscattered light. We emphasize that it is a delicate electromagnetic interaction among (i) localized resonances in single NPs, (ii) collective coupling between NPs (i.e., SLRs), and

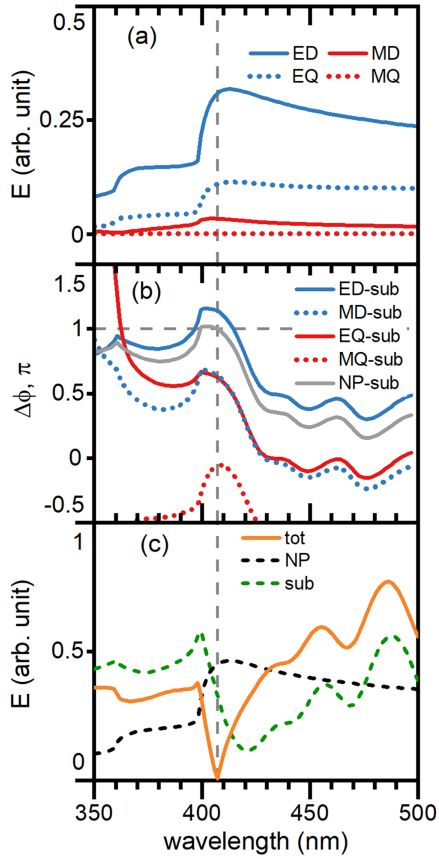

Fig. 4. Detailed analysis of the field scattered from arrays considered in Fig. 3(c): (a) multipole decomposition of the electric field, $|\mathbf{E}|$, induced on NPs; (b) phase difference between multipole contributions (ED, MD, EQ, MQ) in field scattered by NPs and field scattered by a substrate (sub); (c) contributions to the total (tot) electric field from nanoparticles (NP) and substrate (sub).

(iii) field reflected from a substrate, which allows the emergence of the *substrate-mediated* lattice Kerker effect.

C. Sensing Applications

The very presence of a half-space geometry and the existence of a narrowband dip in the reflectance spectra suggest to use considered arrays for sensing purposes [58–61]. Essentially, the sensing mechanism represents a spectral shift of the dip caused by the variation in the refractive index, n_a, of the superstrate (analyte). In our case, the sensitivity is determined as

$$S = \frac{d\lambda_K}{dn_a}, \tag{5}$$

where λ_K is a wavelength of the respective Kerker effect.

It can be seen in Fig. 5 that the change of the refractive index, n_a, of the analyte results in significant variation in the reflectance spectra. For instance, $\lambda_K = 354$ nm for $n_a = 1.33$, and $\lambda_K = 372.4$ nm for $n_a = 1.4$, which results in $S = 263$nm/RIU sensitivity. The Kerker effect emerging in the near UV and blue spectral ranges is promising for application in the spectroscopy of biomaterials with characteristic absorption bands in the respective part of the spectrum [62].

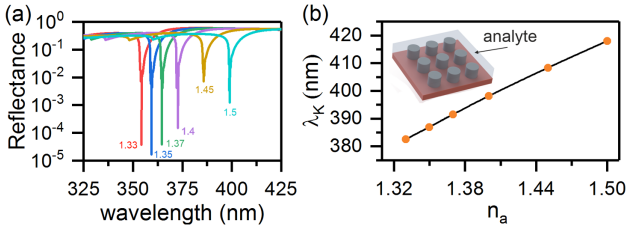

Fig. 5. (a) Reflectance spectra of the structure with fixed $p_y = 240$ nm and $p_x = 265.6$ nm for different values of the analyte refractive index: $n_a = 1.33$, 1.35, 1.37, 1.4, 1.45, and 1.5. (b) Dependence of the Kerker effect wavelength, λ_K, on the refractive index of the analyte, n_a.

4. CONCLUSION

To conclude, we have demonstrated the emergence of the *substrate-mediated* lattice Kerker effect in Al cylindrical NP arrays located on a dielectric substrate. The full suppression of reflection is explained by the destructive interference of electromagnetic waves scattered by NPs and the substrate. It is worth noting that a substrate usually suppresses SLRs, but we show that, on the contrary, the occurrence of a narrowband Kerker effect is possible due to the presence of the substrate. Importantly, in conventional plasmonic (Au, Ag) NPs, the Kerker effect is possible only in the visible and near-infrared spectral ranges [36], while Al NPs have pronounced spectral response in UV range, which allows to use them in a wide variety of applications. For instance, we have shown that the Kerker effect could be used for refractive index sensing applications with ≈ 263nm/RIU sensitivity in the UV spectral range.

Funding. Russian Foundation for Basic Research, Krasnoyarsk Territory and Krasnoyarsk Regional Fund of Science (20-42-240003); Ministry of Science and Higher Education of the Russian Federation (FSRZ-2020-0008).

Disclosures. The authors declare no conflicts of interest.

Data Availability. Data underlying the results presented in this paper are not publicly available at this time but may be obtained from the authors upon reasonable request.

REFERENCES

1. S. Zou and G. C. Schatz, "Narrow plasmonic/photonic extinction and scattering line shapes for one and two dimensional silver nanoparticle arrays," J. Chem. Phys. **121**, 12606–12612 (2004).
2. S. Zou, N. Janel, and G. C. Schatz, "Silver nanoparticle array structures that produce remarkably narrow plasmon lineshapes," J. Chem. Phys. **120**, 10871–10875 (2004).
3. V. A. Markel, "Divergence of dipole sums and the nature of non-Lorentzian exponentially narrow resonances in one-dimensional periodic arrays of nanospheres," J. Phys. B **38**, L115–L121 (2005).
4. B. Auguié and W. L. Barnes, "Collective resonances in gold nanoparticle arrays," Phys. Rev. Lett. **101**, 143902 (2008).
5. Y. Chu, E. Schonbrun, T. Yang, and K. B. Crozier, "Experimental observation of narrow surface plasmon resonances in gold nanoparticle arrays," Appl. Phys. Lett. **93**, 181108 (2008).
6. V. G. Kravets, F. Schedin, and A. N. Grigorenko, "Extremely narrow plasmon resonances based on diffraction coupling of localized plasmons in arrays of metallic nanoparticles," Phys. Rev. Lett. **101**, 087403 (2008).
7. V. O. Byelobrov, T. L. Zinenko, K. Kobayashi, and A. I. Nosich, "Periodicity matters: grating or lattice resonances in the scattering by sparse arrays of subwavelength strips and wires," IEEE Antennas Propag. Mag. **57**(6), 34–45 (2015).

8. M. B. Ross, C. A. Mirkin, and G. C. Schatz, "Optical properties of one-, two-, and three-dimensional arrays of plasmonic nanostructures," J. Phys. Chem. C **120**, 816–830 (2016).
9. V. I. Zakomirnyi, I. L. Rasskazov, V. S. Gerasimov, A. E. Ershov, S. P. Polyutov, and S. V. Karpov, "Refractory titanium nitride two-dimensional structures with extremely narrow surface lattice resonances at telecommunication wavelengths," Appl. Phys. Lett. **111**, 123107 (2017).
10. V. G. Kravets, A. V. Kabashin, W. L. Barnes, and A. N. Grigorenko, "Plasmonic surface lattice resonances: a review of properties and applications," Chem. Rev. **118**, 5912–5951 (2018).
11. I. M. Fradkin, S. A. Dyakov, and N. A. Gippius, "Thickness-independent narrow resonance in a stack of plasmonic lattices," Phys. Rev. Appl. **14**, 054030 (2020).
12. A. D. Utyushev, V. I. Zakomirnyi, and I. L. Rasskazov, "Collective lattice resonances: plasmonics and beyond," Rev. Phys. **6**, 100051 (2021).
13. R. W. Wood, "On a remarkable case of uneven distribution of light in a diffraction grating spectrum," Proc. Phys. Soc. London **18**, 269–275 (1902).
14. L. Rayleigh, "On the dynamical theory of gratings," Proc. R. Soc. A **79**, 399–416 (1907).
15. G. Vecchi, V. Giannini, and J. Gómez Rivas, "Surface modes in plasmonic crystals induced by diffractive coupling of nanoantennas," Phys. Rev. B **80**, 201401 (2009).
16. S. Deng, R. Li, J.-E. Park, J. Guan, P. Choo, J. Hu, P. J. M. Smeets, and T. W. Odom, "Ultranarrow plasmon resonances from annealed nanoparticle lattices," Proc. Natl. Acad. Sci. USA **117**, 23380–23384 (2020).
17. M. S. Bin-Alam, O. Reshef, Y. Mamchur, M. Z. Alam, G. Carlow, J. Upham, B. T. Sullivan, J.-M. Ménard, M. J. Huttunen, R. W. Boyd, and K. Dolgaleva, "Ultra-high-Q resonances in plasmonic metasurfaces," Nat. Commun. **12**, 974 (2021).
18. Z. Li, S. Butun, and K. Aydin, "Ultranarrow band absorbers based on surface lattice resonances in nanostructured metal surfaces," ACS Nano **8**, 8242–8248 (2014).
19. R. R. Gutha, S. M. Sadeghi, and W. J. Wing, "Ultrahigh refractive index sensitivity and tunable polarization switching via infrared plasmonic lattice modes," Appl. Phys. Lett. **110**, 153103 (2017).
20. V. O. Byelobrov, J. Ctyroky, T. M. Benson, R. Sauleau, A. Altintas, and A. I. Nosich, "Low-threshold lasing eigenmodes of an infinite periodic chain of quantum wires," Opt. Lett. **35**, 3634–3636 (2010).
21. V. O. Byelobrov, T. M. Benson, and A. I. Nosich, "Binary grating of subwavelength silver and quantum wires as a photonic-plasmonic lasing platform with nanoscale elements," IEEE J. Sel. Top. Quantum Electron. **18**, 1839–1846 (2012).
22. F. van Beijnum, P. J. van Veldhoven, E. J. Geluk, M. J. A. de Dood, and M. P. van Exter, "Surface plasmon lasing observed in metal hole arrays," Phys. Rev. Lett. **110**, 206802 (2013).
23. J. Zhou, X. Xu, W. Han, D. Mu, H. Song, Y. Meng, X. Leng, J. Yang, X. Di, and Q. Chang, "Fano resonance of nanoparticles embedded in Fabry-Perot cavities," Opt. Express **21**, 12159–12164 (2013).
24. Y. Gao, S. Murai, F. Zhang, S. Tamura, K. Tomita, and K. Tanaka, "Enhancing upconversion photoluminescence by plasmonic-photonic hybrid mode," Opt. Express **28**, 886–897 (2020).
25. Y. Gao, S. Murai, K. Shinozaki, S. Ishii, and K. Tanaka, "Aluminum for near infrared plasmonics: amplified up-conversion photoluminescence from core-shell nanoparticles on periodic lattices," Adv. Opt. Mater. **9**, 2001040 (2021).
26. G. Vecchi, V. Giannini, and J. Gómez Rivas, "Shaping the fluorescent emission by lattice resonances in plasmonic crystals of nanoantennas," Phys. Rev. Lett. **102**, 146807 (2009).
27. S. R. K. Rodriguez, G. Lozano, M. A. Verschuuren, R. Gomes, K. Lambert, B. De Geyter, A. Hassinen, D. Van Thourhout, Z. Hens, and J. G. Rivas, "Quantum rod emission coupled to plasmonic lattice resonances: a collective directional source of polarized light," Appl. Phys. Lett. **100**, 111103 (2012).
28. Y. Kawachiya, S. Murai, M. Saito, K. Fujita, and K. Tanaka, "Photoluminescence decay rate of an emitter layer on an Al nanocylinder array: effect of layer thickness," J. Opt. Soc. Am. B **36**, E1–E8 (2019).
29. S. Murai, M. Saito, Y. Kawachiya, S. Ishii, T. Nakanishi, and K. Tanaka, "Temperature sensing of a plasmonic nanocylinder array by a polymer film containing chameleon complex," J. Opt. Soc. Am. B **36**, E15–E20 (2019).
30. M. Nieto-Vesperinas, R. Gomez-Medina, and J. J. Saenz, "Angle-suppressed scattering and optical forces on submicrometer dielectric particles," J. Opt. Soc. Am. A **28**, 54–60 (2011).
31. J. Geffrin, B. García-Cámara, R. Gómez-Medina, P. Albella, L. Froufe-Pérez, C. Eyraud, A. Litman, R. Vaillon, F. González, M. Nieto-Vesperinas, J. Sáenz, and F. Moreno, "Magnetic and electric coherence in forward- and back-scattered electromagnetic waves by a single dielectric subwavelength sphere," Nat. Commun. **3**, 1171 (2012).
32. V. E. Babicheva and A. B. Evlyukhin, "Resonant lattice Kerker effect in metasurfaces with electric and magnetic optical responses," Laser Photon. Rev. **11**, 1700132 (2017).
33. V. E. Babicheva and J. V. Moloney, "Lattice effect influence on the electric and magnetic dipole resonance overlap in a disk array," Nanophotonics **7**, 1663–1668 (2018).
34. V. E. Babicheva, "Lattice Kerker effect in the array of hexagonal boron nitride antennas," MRS Adv. **3**, 2783–2788 (2018).
35. V. E. Babicheva and A. B. Evlyukhin, "Resonant suppression of light transmission in high-refractive-index nanoparticle metasurfaces," Opt. Lett. **43**, 5186–5189 (2018).
36. V. E. Babicheva and A. B. Evlyukhin, "Metasurfaces with electric quadrupole and magnetic dipole resonant coupling," ACS Photon. **5**, 2022–2033 (2018).
37. V. S. Gerasimov, A. E. Ershov, R. G. Bikbaev, I. L. Rasskazov, I. L. Isaev, P. N. Semina, A. S. Kostyukov, V. I. Zakomirnyi, S. P. Polyutov, and S. V. Karpov, "Plasmonic lattice Kerker effect in ultraviolet-visible spectral range," Phys. Rev. B **103**, 035402 (2021).
38. M. W. Knight, N. S. King, L. Liu, H. O. Everitt, P. Nordlander, and N. J. Halas, "Aluminum for plasmonics," ACS Nano **8**, 834–840 (2014).
39. D. Gérard and S. K. Gray, "Aluminium plasmonics," J. Phys. D **48**, 184001 (2015).
40. A. Yang, A. J. Hryn, M. R. Bourgeois, W.-K. Lee, J. Hu, G. C. Schatz, and T. W. Odom, "Programmable and reversible plasmon mode engineering," Proc. Natl. Acad. Sci. USA **113**, 14201–14206 (2016).
41. D. Khlopin, F. Laux, W. P. Wardley, J. Martin, G. A. Wurtz, J. Plain, N. Bonod, A. V. Zayats, W. Dickson, and D. Gérard, "Lattice modes and plasmonic linewidth engineering in gold and aluminum nanoparticle arrays," J. Opt. Soc. Am. B **34**, 691–700 (2017).
42. M. Esposito, F. Todisco, S. Bakhti, A. Passaseo, I. Tarantini, M. Cuscunà, N. Destouches, and V. Tasco, "Symmetry breaking in oligomer surface plasmon lattice resonances," Nano Lett. **19**, 1922–1930 (2019).
43. X. Zhu, G. M. Imran Hossain, M. George, A. Farhang, A. Cicek, and A. A. Yanik, "Beyond noble metals: high Q-factor aluminum nanoplasmonics," ACS Photon. **7**, 416–424 (2020).
44. A. S. Kostyukov, I. L. Rasskazov, V. S. Gerasimov, S. P. Polyutov, S. V. Karpov, and A. E. Ershov, "Multipolar lattice resonances in plasmonic finite-size metasurfaces," Photonics **8**, 109 (2021).
45. A. E. Ershov, V. S. Gerasimov, R. G. Bikbaev, S. P. Polyutov, and S. V. Karpov, "Mode coupling in arrays of Al nanoparticles," J. Quant. Spectrosc. Radiat. Transfer **248**, 106961 (2020).
46. X. M. Bendaña and F. J. García de Abajo, "Confined collective excitations of self-standing and supported planar periodic particle arrays," Opt. Express **17**, 18826–18835 (2009).
47. B. Auguié, X. M. Bendaña, W. L. Barnes, and F. J. García de Abajo, "Diffractive arrays of gold nanoparticles near an interface: critical role of the substrate," Phys. Rev. B **82**, 155447 (2010).
48. S.-Q. Li, W. Zhou, D. Bruce Buchholz, J. B. Ketterson, L. E. Ocola, K. Sakoda, and R. P. H. Chang, "Ultra-sharp plasmonic resonances from monopole optical nanoantenna phased arrays," Appl. Phys. Lett. **104**, 231101 (2014).
49. S. M. Sadeghi, R. R. Gutha, and W. J. Wing, "Turning on plasmonic lattice modes in metallic nanoantenna arrays via silicon thin films," Opt. Lett. **41**, 3367–3370 (2016).
50. X. Huang, C. Lou, and H. Zhang, "Experimentally demonstrating plasmonic lattice mode in periodic Ag nanoparticle arrays on quartz trapezoidal pillars," J. Phys. D **51**, 465101 (2018).

51. K. V. Baryshnikova, M. I. Petrov, V. E. Babicheva, and P. A. Belov, "Plasmonic and silicon spherical nanoparticle antireflective coatings," Sci. Rep. **6**, 22136 (2016).
52. D. Smith, E. Shiles, and M. Inokuti, "The optical properties of metallic aluminum," in *Handbook of Optical Constants of Solids*, E. D. Palik, ed. (Academic, 1997), pp. 369–406.
53. Lumerical Solutions, FDTD Solutions (2020).
54. L. D. Landau and E. M. Lifshitz, *The Classical Theory of Fields*, 4th ed., Vol. **2** of Course of Theoretical Physics (Butterworth-Heinemann, 1987).
55. P. D. Terekhov, V. E. Babicheva, K. V. Baryshnikova, A. S. Shalin, A. Karabchevsky, and A. B. Evlyukhin, "Multipole analysis of dielectric metasurfaces composed of nonspherical nanoparticles and lattice invisibility effect," Phys. Rev. B **99**, 045424 (2019).
56. J. Li, N. Verellen, and P. Van Dorpe, "Engineering electric and magnetic dipole coupling in arrays of dielectric nanoparticles," J. Appl. Phys. **123**, 083101 (2018).
57. V. I. Zakomirnyi, S. V. Karpov, H. Ågren, and I. L. Rasskazov, "Collective lattice resonances in disordered and quasi-random all-dielectric metasurfaces," J. Opt. Soc. Am. B **36**, E21–E29 (2019).
58. S. Enoch, R. Quidant, and G. Badenes, "Optical sensing based on plasmon coupling in nanoparticle arrays," Opt. Express **12**, 3422–3427 (2004).
59. V. G. Kravets, F. Schedin, A. V. Kabashin, and A. N. Grigorenko, "Sensitivity of collective plasmon modes of gold nanoresonators to local environment," Opt. Lett. **35**, 956–958 (2010).
60. B. D. Thackray, V. G. Kravets, F. Schedin, G. Auton, P. A. Thomas, and A. N. Grigorenko, "Narrow collective plasmon resonances in nanostructure arrays observed at normal light incidence for simplified sensing in asymmetric air and water environments," ACS Photon. **1**, 1116–1126 (2014).
61. L. Y. M. Tobing, A. M. Soehartono, A. D. Mueller, K.-T. Yong, W. Fan, and D. H. Zhang, "Hybridized surface lattice modes in intercalated 3-disk plasmonic crystals for high figure-of-merit plasmonic sensing," Nanoscale **13**, 4092–4102 (2021).
62. I. Tanabe, Y. Y. Tanaka, K. Watari, T. Hanulia, T. Goto, W. Inami, Y. Kawata, and Y. Ozaki, "Aluminum film thickness dependence of surface plasmon resonance in the far- and deep-ultraviolet regions," Chem. Lett. **46**, 1560–1563 (2017).